Dark-ISP: Enhancing RAW Image Processing for Low-Light Object Detection

Jiasheng Guo[1,*] Xin Gao[1,*] Yuxiang Yan[1] Guanghao Li[1] Jian Pu[1,†]
[1] Institute of Science and Technology for Brain-inspired Intelligence, Fudan University
{guojs22, gaoxin23, yxyan22, ghli22}@m.fudan.edu.cn, {jianpu}@fudan.edu.cn

Abstract

Low-light Object detection is crucial for many real-world applications but remains challenging due to degraded image quality. While recent studies have shown that RAW images offer superior potential over RGB images, existing approaches either use RAW-RGB images[1] with information loss or employ complex frameworks. To address these, we propose a lightweight and self-adaptive Image Signal Processing (ISP) plugin, ***Dark-ISP****, which directly processes Bayer RAW images in dark environments, enabling seamless end-to-end training for object detection. Our key innovations are: (1) We deconstruct conventional ISP pipelines into sequential linear (sensor calibration) and nonlinear (tone mapping) sub-modules, recasting them as differentiable components optimized through task-driven losses. Each module is equpped with content-aware adaptability and physics-informed priors, enabling automatic RAW-to-RGB conversion aligned with detection objectives. (2) By exploiting the ISP pipeline's intrinsic cascade structure, we devise a Self-Boost mechanism that facilitates cooperation between sub-modules. Through extensive experiments on three RAW image datasets, we demonstrate that our method outperforms state-of-the-art RGB- and RAW-based detection approaches, achieving superior results with minimal parameters in challenging low-light environments.*

1. Introduction

Object detection in low-light conditions is vital for applications such as autonomous driving and surveillance [5, 24, 38, 45]. However, darkness induces severe image degradation characterized by noise amplification and diminished contrast, thereby posing substantial challenges to detection algorithms. Traditional methods using compressed dynamic range RGB images are limited by the low-bit-depth information and noise introduced during image signal processing (ISP), significantly reducing their effectiveness in low-light environments [36, 46, 57, 58].

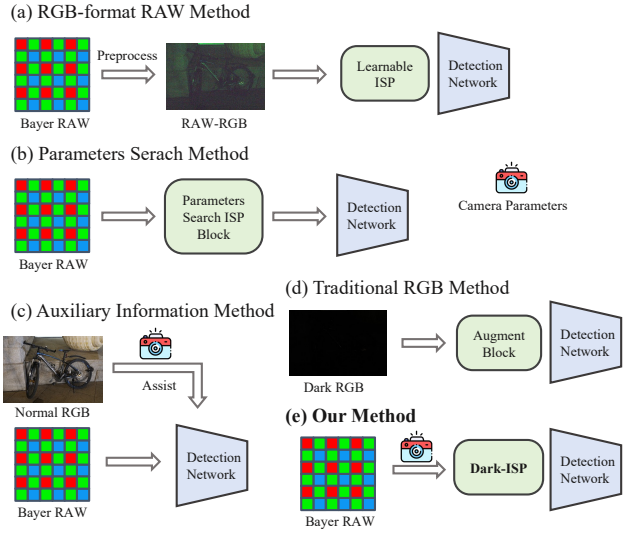

Figure 1. Thumbnails of different low-light object detection pipelines. (a) Methods utilizing RAW-RGB data. (b) ISP parameter search methods. (c) Methods incorporating auxiliary information for training. (d) Dark RGB image enhancement pipeline. (e) Our proposed Dark-ISP.

Unlike RGB images, RAW images directly capture sensor orignal data before ISP processing, preserving physically meaningful information such as scene radiance and noise characteristics [53, 54]. This results in RAW images containing richer details and color information compared to RGB images, offering greater flexibility in post-processing. Furthermore, RAW format files also store camera metadata during the photography process, which can serve as auxiliary information to provide additional guidance for deep network training.

Effectively and efficiently utilizing the rich information in RAW images for object detection remains a significant challenge. Existing methods to bridging the RAW image and downstream networks pretrained on RGB domain can

*These authors contributed equally to this work.
†Corresponding author.
[1] In this paper, we use raw Bayer sensor data directly, while some methods quantize high-bit-depth 'Bayer RAW' into 'RAW-RGB' images with 8 bit-depth[10, 15]. We distinguish between these two terms.

be broadly classified into three categories. The first approach (Fig. 1(a)) bining and quantize four-channel Bayer RAW images into three-channel RAW-RGB to ensure compatibility with pretrained backbone, as seen in LIS [10], Crafting [30], and RAW-Adapter [15]. However, this conversion reduces bit-depth and leads to substantial information loss, limiting the benefits of RAW data. The second approach (Fig. 1(b)) incorporates parameters searching ISP, such as NOD [41], AdaptiveISP [52], Qin *et al.*[44], and DynamicISP [60] which directly process Bayer RAW images using trainable ISP modules to bridge the RAW and RGB domains. While effective, these methods often introduce computationally expensive processes, such as complex parameter searching algorithms and multi-stage training strategy, making them impractical for real-world deployment. The third category (Fig. 1(c)) relies on auxiliary information augmentation, where methods like ISP-Teacher [66] and Multitask AET [16] integrate normal-light RGB or camera metadata references during training, but the requirement for such additional data may not always be necessary.

To address these limitations, we propose **Dark-ISP**, a lightweight and self-adaptive ISP plugin that fully exploits the advantages of RAW images for low-light object detection. By analyzing the sequential steps of camera ISP, we design a decoupled framework consisting of linear and nonlinear components. The **linear component** captures fundamental camera operations through a sequence of matrix operations, enhanced by Local-Global Attention to dynamically balance sensor-derived processes with scene patterns. For the **nonlinear component**, inspired by the tone mapping function's ability to stretch dark regions and compress bright areas, we define a set of non-convex polynomial bases with strong physical interpretability. Instead of learning arbitrary transformations, our method learns the coefficients to combine these bases into an effective nonlinear operation. To encourage synergy between these two submodules, we also introduce a **Self-Boost Regularization** that uses the output of the nonlinear component to guide the learning direction of the linear mapping. Extensive validation across both real-world and synthetic RAW datasets demonstrates that our approach outperforms previous RGB-RAW methods, exhibiting superior generalization ability.

The main contributions of this work are as follows:

- We propose a lightweight ISP plugin that separates linear and nonlinear processing, integrating content-aware adaptability and physics-informed priors to fully exploit Bayer RAW image for low-light object detection.
- We propose a Self-Boost mechanism that enhances synergy between sub-modules in the ISP, improving robustness across varying lighting conditions.
- We demonstrate superior performance over existing methods with fewer parameters on three low-light RAW image object detection datasets.

2. Related Work

2.1. Low-light Object Detection

Low-light object detection remains a challenging task due to weak illumination and noise degradation. Existing methods can be broadly categorized into image-level and feature-level approaches. *Image-level methods* process images prior to detection through illumination enhancement [26, 57] and noise suppression [28, 43]. For example, FeatEnHancer [28] hierarchically combines multiscale features to enhance the image before downstream network. *Feature-level methods* focus on designing specialized modules and learning strategies to extract clean, informative features [21, 36]. *Hybrid approaches* [14, 43, 58] integrate the above two categories into a unified framework, enabling synergistic interaction. For instance, contrastive learning [58] jointly optimizes both components to enhance image quality and detection performance. While existing works have achieved promising results, they predominantly operate on processed RGB images that inherently suffer from information loss and compound noise introduced in the ISP. Recent attempts [10, 30] use quantized RAW data, which reduces bit-depth and loses sensor-specific information, making them less robust. We argue that *unquantized Bayer RAW images* retain superior photonic information and dynamic range, motivating our framework to directly leverage RAW sensor data for end-to-end low-light object detection and bypass the information bottleneck of RGB-based approaches.

2.2. Image Signal Processing

Image Signal Processing (ISP) transforms RAW sensor data into high-quality images. Traditional ISP methods rely on manually designed components executed sequentially [18, 22, 34, 67]. Recently, deep learning has been incorporated into ISP, with two main strategies: *Image-to-image frameworks* focus on learning the mapping from RAW to RGB images. Differentiable modules have been introduced into the ISP pipeline, enabling end-to-end optimization for high-quality image generation [25, 33, 35, 40]. Symmetric bidirectional structures [2, 55, 61] also have been proposed to learn reversible mappings between RAW and sRGB images, facilitating reversible conversion and preserving more information from the original RAW data. To improve color manipulation, lookup tables (LUTs) [13, 49, 59, 62] have been integrated with deep networks to efficiently retrieve pixel color values through lookup and interpolation operations. *Task-driven ISP optimization* directly adjusts ISP parameters based on task-specific objectives. GenISP [41] and Guo *et al.* [27] adopt multi-stage training to align ISP outputs with downstream network requirements. Several methods refine ISP components using reinforcement learning for adaptive search [51] or gradient-based optimization guided by task losses [42, 44, 60]. ISP-teacher [66] improves ro-

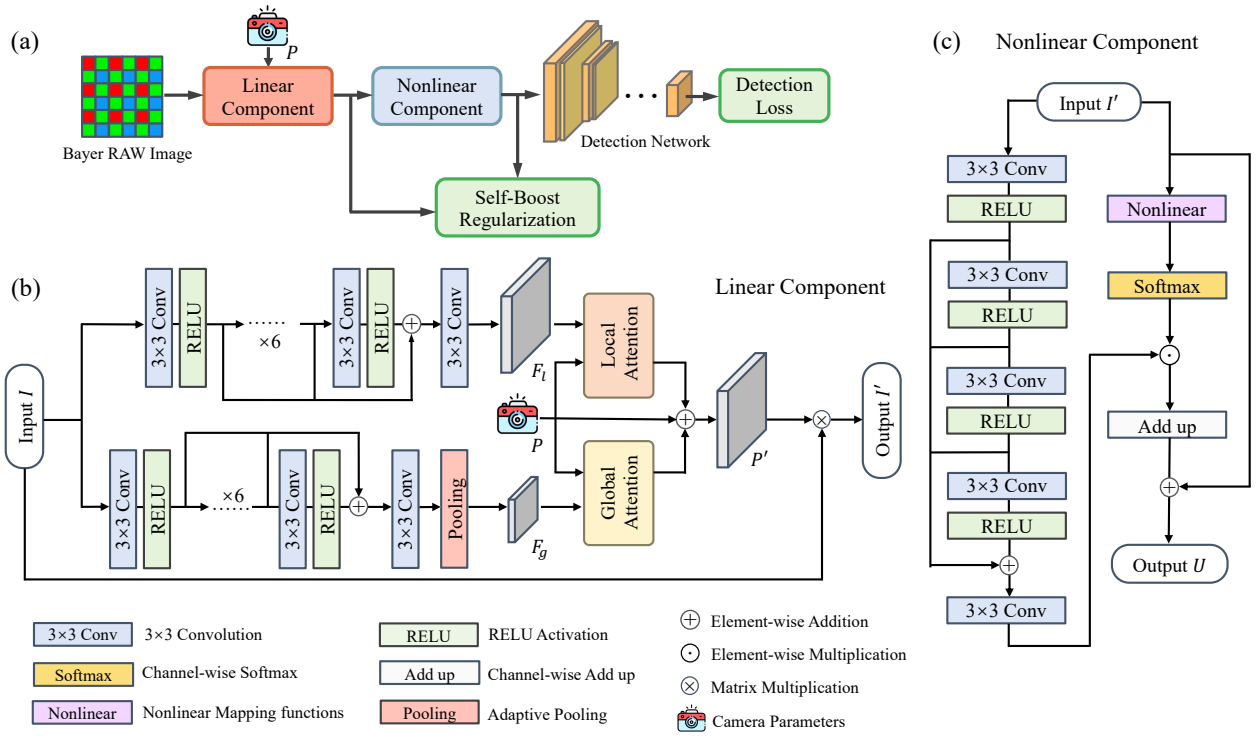

Figure 2. (a) Overview of Dark-ISP. The linear and nonlinear components process Bayer-format inputs I sequentially, with the Self-Boost Regularization $\mathcal{L}_{sb}$ guiding the learning of the linear component. (b) **Linear Component**: P is the camera parameter matrix. F_l and F_g represent the local and global features, which produce context-aware matrices via the Attention mechanism, combined to form an adaptive linear transformation P'. (c) **Nonlinear Component**: The image I' from the Linear Component is passed through a network to generate pixel-wise coefficient maps, combined with predefined bases for the nonlinear transformation.

bustness by leveraging well-lit RGB images as auxiliary inputs. RAW-Adapter [15] introduces learnable queries to refine ISP parameters and enable interaction with downstream networks. Compared to these studies, our design streamlines both training and deployment through its straightforward architecture.

2.3. Low-Light RAW Image Enhancement

The potential of RAW images for low-light enhancement was first highlighted by SID [6], sparking subsequent research to bypass the RGB domain and directly process RAW images. Some methods [4, 23, 32, 53, 63, 65] develop noise models for dark RAW images, replacing traditional Gaussian models with more accurate CMOS sensor-based approaches for noise removal. Other works [7, 19, 20, 31, 39] utilize heuristic frameworks and advanced network designs [8, 11, 56] to directly map noisy to clean RAW images. Recently, techniques like Diffusion [17, 50] and Mamba [12] have also been explored for RAW image enhancement. However, these approaches focus primarily on image-level enhancement without integrating downstream tasks. In contrast, our method connects RAW images directly to downstream object detection tasks, enabling end-to-end training through a mediating ISP structure that bridges the RAW and RGB domains.

3. Method

We present the Dark-ISP framework in Fig. 2. Following the conventional camera ISP pipeline, the RAW images first pass through the linear mapping module (Sec. 3.1), which enhances standard camera operations with a context-aware attention mechanism. The nonlinear component (Sec. 3.2) then applies a set of concave function bases to model effective nonlinear transformations. To promote synergy between these components, we introduce a Self-Boost Regularization loss (Sec. 3.3) that aligns their optimization.

3.1. Dynamic Linear Mapping

In traditional ISP pipelines, operations like *White Balance*, *Binning*, and *Color Space Transform* are performed sequentially as linear processes [18]. These steps adjust color balance, convert Bayer images $I \in \mathbb{R}^{4\times H\times W}$ to RGB, and map RAW sensor data to a perceptually uniform color space using matrix transformations.

First, the *White Balance* operation compensates for light source variations by applying a diagonal gain matrix $W \in$

$\mathbb{R}^{4\times4}$ to the RAW data:

$$\begin{pmatrix} r' \\ g'_r \\ b' \\ g'_b \end{pmatrix} = \begin{pmatrix} w_1 & 0 & 0 & 0 \\ 0 & w_2 & 0 & 0 \\ 0 & 0 & w_3 & 0 \\ 0 & 0 & 0 & w_4 \end{pmatrix} \cdot \begin{pmatrix} r \\ g_r \\ b \\ g_b \end{pmatrix}. \tag{1}$$

Next, the *Binning* operation merges the four Bayer channels into three RGB channels, averaging the two green channels using the sparse matrix $B \in \mathbb{R}^{3\times4}$:

$$\begin{pmatrix} R \\ G \\ B \end{pmatrix} = \begin{pmatrix} 1 & 0 & 0 & 0 \\ 0 & \frac{1}{2} & 0 & \frac{1}{2} \\ 0 & 0 & 1 & 0 \end{pmatrix} \cdot \begin{pmatrix} r' \\ g'_r \\ b' \\ g'_b \end{pmatrix}. \tag{2}$$

Following this, the *Color Space Transform* step uses a color correction matrix $C \in \mathbb{R}^{3\times3}$ to map the image to a perceptual color space: [18]:

$$\begin{pmatrix} R' \\ G' \\ B' \end{pmatrix} = \begin{pmatrix} c_{11} & c_{12} & c_{13} \\ c_{21} & c_{22} & c_{23} \\ c_{31} & c_{32} & c_{33} \end{pmatrix} \cdot \begin{pmatrix} R \\ G \\ B \end{pmatrix}. \tag{3}$$

The entire process can be compactly summarized as a single matrix $P \in \mathbb{R}^{3\times4}$ that transforms the RAW image I into the corrected RGB image $I' \in \mathbb{R}^{3\times H\times W}$:

$$I' = C \cdot B \cdot W \cdot I = P \cdot I. \tag{4}$$

The white balance coefficients and the CCM are typically determined through automatic white balance algorithms in the camera, as well as manual regression estimates against standard colors [18]. Since these parameters are specific to each camera, they remain largely static within the image processing pipeline. To improve the communication between the image, downstream tasks, and these parameters, we treat them as part of the learning process.

To enhance adaptability across sensors and low-light conditions, we introduce a dynamic mapping. Inspired by hierarchical feature extractors [3, 47, 64, 68], the RAW image I is first processed through a dual-stream architecture to extract pixel-level local features $F_l \in \mathbb{R}^{C\times H\times W}$ and image-level global features $F_g \in \mathbb{R}^{C\times\frac{H}{16}\times\frac{W}{16}}$, which are then used in Local and Global Attention mechanisms [48] to generate pixel-level and image-level operations:

$$\begin{aligned} P_l &= \text{LocalAttn}(Q = F_l, K = P, V = P) \in \mathbb{R}^{(3\times4)\times H\times W} \\ P_g &= \text{GlobalAttn}(Q = P, K = F_g, V = F_g) \in \mathbb{R}^{3\times4}. \end{aligned} \tag{5}$$

The local and global operations are then combined using an arithmetic sum (broadcasting) with a skip connection to produce the adaptive linear transformation $P' = (P_l + P_g + P) \in \mathbb{R}^{3\times4\times H\times W}$. These parameters are applied to the RAW image to produce the corrected RGB output:

$$I' = (P_l + P_g + P) \cdot I = P' \cdot I. \tag{6}$$

This process is driven by both photographic principles and task-specific feedback, enabling a flexible, content-aware transformation that enhances performance under low-light conditions, particularly for object detection.

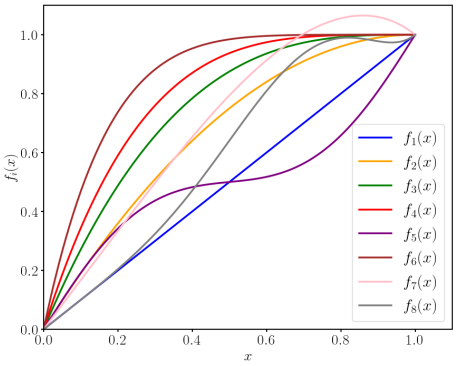

Figure 3. Non-convex polynomial bases from first-order to eighth-order. f_k represents the polynomial of order k.

3.2. Nonlinear Stretch with Polynomial Bases

The nonlinear component of the Image Signal Processor (ISP) is crucial for adjusting the RGB image's color distribution. It enhances visual aesthetics and supports pixel-wise operations such as denoising and sharpening. Rather than relying on a black-box neural network transformation, we explicitly design **physically interpretable function bases** to ensure the desired properties and adaptively combine them for image-specific enhancement.

For each image I' produced by the linear module, a network predicts pixel-wise coefficients $\{C_k\}_{k=0}^n$. These coefficients are then combined with a set of polynomial bases $\{f_k(x)\}_{k=0}^n$ to form the nonlinear transformation:

$$\mathcal{F}(x_{ij}) = \sum_{k=0}^{n} C_k(i,j) f_k(x_{ij}). \tag{7}$$

Here, (i, j) represents the pixel position. This transformation can approximate a complex, locally smooth function $\mathcal{H}(\cdot)$ with high-order infinitesimal errors $o(x^n)$:

$$\mathcal{H}(x) = \mathcal{F}(x) + o(x^n) = \sum_{k=0}^{n} C_k(i,j) f_k(x) + o(x^n). \tag{8}$$

This is analogous to an n-order Taylor expansion, where terms are reordered and coefficients combined.

To design the bases that govern the nonlinear transformation, we focus on addressing low-light image behavior. Under such conditions, non-convex mappings are required to stretch the dark regions while compressing the bright areas. This adjustment enhances shadow details and prevents overexposure in bright regions—critical for improving visual quality. To this end, we design a set of non-convex bases with $f_0 = 1$ and each $f_k(x)$ is a polynomial of order k that passes through the points $(0, 0)$ and $(1, 1)$. These polynomials capture varying curvature patterns, from nearly linear to concave, effectively handling intensity redistribution in low-light scenarios, as shown in Fig. 3. The set of

polynomial bases thus forms a low-dimensional manifold of valid tone-mapping operations $\mathcal{F}(\cdot)$.

Importantly, it is not an error-prone approximation for us to use $\mathcal{F}(\cdot)$; instead, it constrains the nonlinear function to a finite n-dimensional polynomial, leveraging prior knowledge to balance expressiveness and computational efficiency. The transformed $U = \mathcal{F}(I')$ provides the enhanced image for downstream tasks.

Our method shares similarities with Zero-DCE [25], which also uses a neural network to generate coefficients for quadratic curve fitting. However, our approach differs by explicitly considering low-light behavior, preventing suboptimal convergence. Specifically, we use 3×3 convolution layers to predict pixel-wise coefficient maps $\{C_k\}_{k=0}^{n}$, which are then combined with the polynomial bases (as shown in Fig. 2 (c)). To prevent gradient vanishing, skip connections are used, and x is subtracted from the original polynomial function to preserve the curve's shape.

3.3. Self-Boost Regularization

To enhance the compatibility between linear and nonlinear components in Sec. 3.1-3.2, we propose a Self-Boost regularization mechanism. Given the linearly transformed image $I' = P' \cdot I$ from the RAW Bayer input I, the nonlinear module generates the enhanced image $U = \mathcal{F}(I')$.

Ideally, given an oracle sRGB image $U^* \in \mathbb{R}^{3\times H\times W}$ captured under normal lighting conditions, the optimal linear mapping can be found via the closed-form least squares solution:

$$P^* = \arg\min_{P'} \|U^* - P' \cdot I\|^2 = U^* \cdot I^T \cdot (I \cdot I^T)^{-1}, \quad (9)$$

where $P^* \in \mathbb{R}^{3\times 4}$ and all images are reshaped into matrices of size $[C \times (H \times W)]$. However, this ideal formulation requires paired RAW-sRGB samples (I, U^*), the acquisition of which is prohibitive expensive.

As a relaxation, we propose a self-supervised approximation by substituting the oracle U^* with the nonlinear module's own output, U. This is motivated by the intrinsic feature hierarchy hypothesis, which suggests that deeper network layers produce representations closer to the final objective than shallow layers [1]. Critically, because U is a function of P', the closed-form solution in Eq. (9) is no longer holds when substituting U for U^*. Nevertheless, our objective is to encourage the linear component's output, $P' \cdot I$, to closely approximate the nonlinear output, U. We therefore treat U as a pseudo-target and define an approximate linear mapping $\tilde{P}$ as follows:

$$\tilde{P} := U \cdot I^T \cdot (I \cdot I^T)^{-1}. \quad (10)$$

This formulation serves a dual purpose: it facilitates a more effective backpropagation of gradients from the high-level detection loss to the linear component P', while also providing U with greater optimization potential in the adversarial process of this regularization and detection loss. We verify the validity of these properties in the appendix.

A direct alignment between P' and $\tilde{P}$ is inappropriate because $\tilde{P}$ is merely an approximation of the solution P^* and both matrices are continuously updated during training. Therefore, instead of enforcing a strict equality, we encourage directional consistency between the corresponding row vectors of P' and $\tilde{P}$. We decompose each matrix into its constituent row vectors, $P' = (\mathbf{p'_1}, \mathbf{p'_2}, \mathbf{p'_3})^T$ and $\tilde{P} = (\tilde{\mathbf{p}}_\mathbf{1}, \tilde{\mathbf{p}}_\mathbf{2}, \tilde{\mathbf{p}}_\mathbf{3})^T$, where each vector represents the linear projection from the four Bayer channels to a single RGB channel. Our Self-Boost loss, $\mathcal{L}_{sb}$, is then defined as the sum of the cosine distances between these corresponding vector pairs:

$$\mathcal{L}_{sb} = \sum_{\mathbf{p'_i}\in P',\, \tilde{\mathbf{p}}_\mathbf{i}\in\tilde{P}} \|\mathbf{1} - \cos(\mathbf{p'_i}, \tilde{\mathbf{p}}_\mathbf{i})\|. \quad (11)$$

To prevent premature convergence, we activate $\mathcal{L}_{sb}$ after N warmup epochs. The compound loss integrates with detection supervision as:

$$\mathcal{L} = \mathcal{L}_{det} + \lambda \cdot \mathcal{L}_{sb}, \quad (12)$$

where λ is empirically set to 1×10^{-2} for all experiments.

4. Experiments

Implementation Details. Our framework is based on the MMDetection toolbox [9] and runs on a Tesla-V100 32GB GPU. For object detection, we use the RetinaNet detector [38] with a ResNet [29] backbone initialized with ImageNet pre-trained weights. The model is trained with the SGD optimizer with an initial learning rate of 0.001, momentum of 0.9, and weight decay of 0.0001 for 15 epochs across all datasets. Random horizontal flipping is applied as augmentation, and all images are resized to 400×600. We choose the order $n = 8$ for the nonlinear component in Sec. 3.2.

Datasets and Metrics. We evaluate our method on two real-world RAW datasets, LOD [30] and NOD [41], and a synthetic dataset, SynCOCO [37]. **The LOD dataset** contains 2,230 low-light RAW images from a Canon EOS 5D Mark IV, spanning 8 object classes. We use 1,800 for training and 430 for testing, evaluating performance with VOC-style mAP. **The NOD dataset** consists of RAW images captured in low-light environments with two cameras (Sony RX100 VII and Nikon D750), containing 3 object classes. The Sony dataset has 2,751 training and 321 test images, while the Nikon dataset has 3,206 training and 400 test images. In both datasets, each Bayer RAW image (.NEF, .ARW) is demosaiced into four RGBG channels, and resized to match the size of RGB images before being fed into the model. Performance is evaluated using COCO-style mAP, mAP_{50}, and mAP_{75}.

Table 1. Detection performance comparison on the real-world LOD dataset. **Bold** indicates the best result, and underline indicates the second best. $*$ denotes a two-stage training method.

Image Format	Method	ResNet18 mAP	ResNet50 mAP
RGB RAW-RGB	default ISP	55.2	59.1
	demosaic	52.6	61.3
	LIS [10]	50.5	60.8
	FeatEnHancer [28]	60.8	64.3
	RAW-Adapter [15]	55.4	61.1
Bayer RAW	default ISP	63.6	67.3
	demosaic	59.7	65.1
	LIS [10]	58.4	67.9
	SID* [6]	61.2	64.7
	FeatEnHancer [28]	63.4	67.0
	RAW-Adapter [15]	59.9	66.2
	Our Dark-ISP	**64.9**	**70.4**

Table 2. Detection performance comparison on the NOD dataset using RAW images captured in low-light conditions with two cameras: Sony RX100 VII 320 and Nikon D750.

Camera	Method	mAP	mAP_{50}	mAP_{75}
Sony	default ISP	28.3	51.0	29.2
	demosaic	19.7	40.0	18.4
	LIS [10]	28.3	48.3	29.7
	SID* [6]	27.4	47.2	28.2
	FeatEnHancer [28]	30.3	52.1	31.5
	RAW-Adapter [15]	28.9	50.7	29.6
	Dark-ISP(Ours)	**31.5**	**53.4**	**32.2**
Nikon	default ISP	27.4	47.5	28.5
	demosaic	27.6	48.6	27.8
	LIS [10]	26.5	46.4	27.4
	SID*[6]	22.2	42.0	20.5
	FeatEnHancer [28]	28.8	48.9	**30.8**
	RAW-Adapter [15]	28.3	48.2	28.7
	Our Dark-ISP	**29.9**	**50.9**	30.7

Additionally, we generated a **synthetic COCO RAW dark dataset** using the widely used COCO dataset [37]. Following the pipeline from LIS [10], we first apply the inverse ISP process to normal-light RGB images to generate synthetic RAW images. Dark noise from the physical noise model [53, 54] is then injected to simulate dark RAW images. The same metrics as those used in COCO are applied for training and evaluation.

4.1. Comparison with State-of-the-Art Methods

We compare Dark-ISP with the original Dark RGB and RAW images as well as several state-of-the-art methods: SID [6], FeatEnHancer [28], LIS [10], and RAW-Adapter [15]. Dark RGB images are obtained through the ISP pipeline in LED [32] and are represented as "default ISP" in the experiment. Dark RAW images, which only undergo demosaicing and binning operations, are called "demosaic". SID, a pioneering dark RAW image denoising approach, requires a pre-trained denoising network before object detection tasks. FeatEnHancer is an end-to-end module for enhancing dark RGB images in perceptual tasks. LIS and RAW-Adapter are end-to-end methods that process RAW-RGB images. All methods were evaluated using the same data augmentation and training configurations for a fair comparison.

Table 3. Detection performance comparison on the SynCOCO dataset, a synthetic RAW dark dataset with a larger sample size.

Input Format	Method	mAP	mAP_{50}	mAP_{75}
RGB RAW-RGB	default ISP	21.4	34.5	22.9
	demosaic	19.6	31.7	20.5
	LIS [10]	16.5	17.7	17.5
	FeatEnHancer [28]	21.3	34.4	21.8
	RAW-Adapter [15]	21.0	34.3	22.1
Bayer RAW	default ISP	21.5	35.9	23.1
	demosaic	21.0	34.1	22.8
	LIS [10]	21.4	34.5	23.1
	SID* [6]	21.2	34.6	22.6
	FeatEnHancer [28]	22.4	36.1	23.9
	RAW-Adapter [15]	21.7	34.9	23.1
	Our Dark-ISP	**23.1**	**37.7**	**24.4**

4.1.1. Quantitative Analysis

The detection performance on the LOD dataset is illustrated in Tab. 1. Our evaluation utilized two backbone depths (ResNet-18 and ResNet-50) to assess scalability. Inputs included both **Bayer RAW**, **RAW-RGB** and **RGB** images (low-bit-depth compressed versions of Bayer images), enabling a comparative study of image format impacts. As seen in the results, input from the Bayer RAW outperforms RGB or RAW-RGB images across most methods, highlighting that direct sensor data provides richer information. Compared to other methods, our approach achieved the best results on both sizes of backbones (**64.9 mAP** and **70.4 mAP**), highlighting its ability to better leverage and extract useful information from Bayer RAW inputs in dark environment. It is important to note that SID, as a two-stage method, effectively reduces dark noise but shows minimal improvement in performance. This suggests that, for downstream tasks, the ability to adapt the RAW image distribution to the pre-trained backbone is crucial for achieving optimal performance. Furthermore, when using Bayer RAW as input, the basic camera default ISP performs on par with other learnable methods, indicating significant untapped potential in Bayer RAW inputs.

To evaluate the generalization of our method, we tested

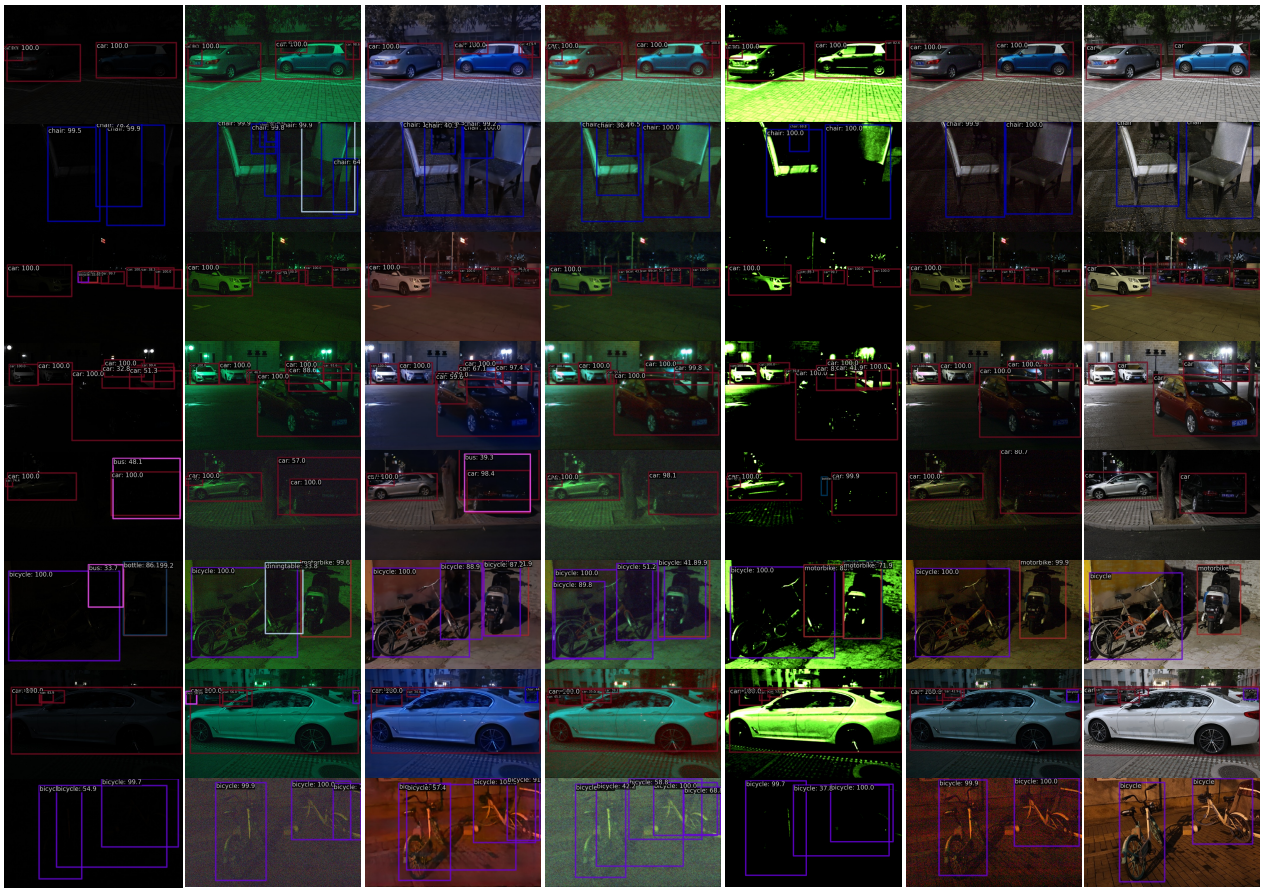

Figure 4. Visual comparisons on the LOD dataset. Results are shown on the enhanced images before being fed into the detection network backbone for each method. Our method outperforms others in minimizing missed and false detections, please zoom in for details.

it on the NOD dataset (see Tab. 2). Our approach outperformed others on data from both Sony and Nikon cameras, demonstrating its robustness across diverse camera parameters and its ability to adapt to each camera's characteristics using task-specific losses.

Finally, the results on the SynCOCO dataset, presented in Tab. 3, further validate the effectiveness of our method even when trained with a larger dataset. Despite significant differences between synthetic RAW images obtained through inverse ISP processing and real RAW images, the addition of extra channels provides the model with more data to learn from, and our method continues to effectively capture this information.

4.1.2. Qualitative Analysis

Qualitative results on the LOD dataset, as shown in Fig. 4, demonstrate that the proposed method consistently recalls most of the targets, even in challenging scenarios. Our approach excels at accurately detecting objects in dark environments compared to other methods. In terms of visual quality, the images enhanced by our proposed ISP are closer to the ground-truth normal RGB images, indicating that it has successfully learned the necessary transformations to align RAW domain images with the RGB domain of the pre-trained backbone.

The results on the NOD dataset, visualized in Fig. 5 and Fig. 6, further emphasize the effectiveness of our method. Compared to two competitive approaches, our method reliably detects objects in dark regions across both camera datasets, avoiding false positives and missed detections. This underscores the superiority of our approach in detecting objects under low-light conditions and its robustness across different camera setups.

4.2. Ablation Study

We conduct a series of ablation experiments on the LOD dataset to investigate the impact of the modules in the proposed pipeline on object detection in dark environments.

As shown in Tab. 4, the three modules in the pipeline serve distinct roles. The nonlinear component, due to its

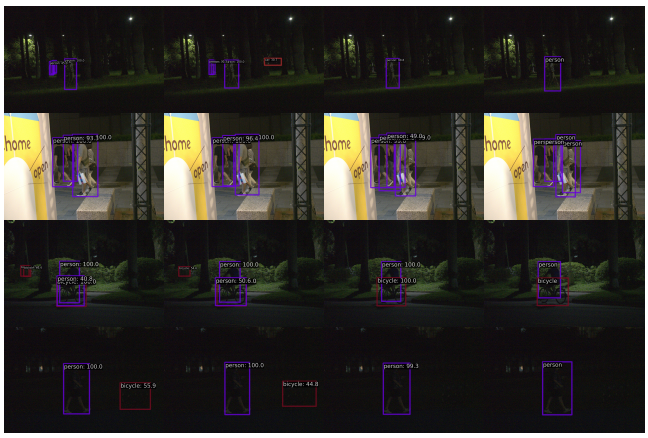

FeatEnHancer RAW-Adapter **Our Dark-ISP** Ground Truth

Figure 5. Visual comparison of our method with the two top-performing competitors on the NOD dataset (Sony camera).

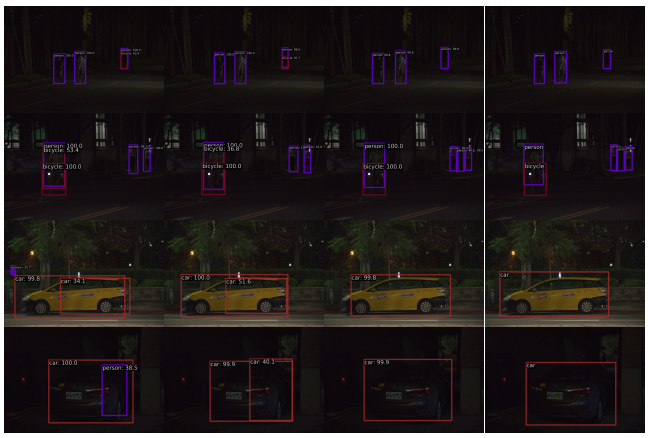

FeatEnHancer RAW-Adapter **Our Dark-ISP** Ground Truth

Figure 6. Visual comparison of our method with the two top-performing competitors on the NOD dataset (Nikon camera).

non-convex nature, better adapts image pixel distributions for dark perception tasks, outperforming the linear component. When combined, the two components exceed their individual performances. The Self-Boost mechanism enhances module interaction, improving information extraction from RAW images and boosting detection accuracy to 70.4 mAP.

For the linear component, we compared using fixed parameters from the traditional ISP, as well as using only local or global information. By introducing only a small number of parameters (0.345MB), it outperforms the Default ISP by 4 mAP in low-light detection. All results and detailed analysis can be found in the supplementary material.

The nonlinear component plays a crucial role in tone mapping and adjusting image distribution for downstream detection tasks. There are several design alternatives for this component, which we evaluate in this study. First, we use gamma correction from traditional ISP as the baseline and compare it with the learnable gamma values (Gamma†) [40] and a 3D color lookup table (LUT) method [62]. Additionally, we examine ResMLP, the color manipulation technique used in RAW-Adapter [15]. As shown in Tab. 5, our method outperforms the alternatives even without the skip connection, by leveraging a non-convex prior that is well-suited for low-light conditions. When the skip connection is added, it mitigates the vanishing gradient problem, allowing our method to achieve the best performance while maintaining a relatively small number of parameters.

Table 4. Ablation study of the proposed pipeline.

Linear	Nonlinear	Self-Boost Regularization	mAP
✓			66.6
	✓		67.1
✓	✓		68.7
✓	✓	✓	**70.4**

Table 5. Ablation study for Nonlinear component. w/o Skip means the removal of the skip connection in the Nonlinear Component.

Method	mAP	Param(MB)
Gamma	66.4	-
Gamma† [40]	68.0	-
LUT [62]	67.8	0.192
ResMLP [15]	67.0	0.049
Zero-DCE [25]	68.0	0.304
Ours w/o Skip	<u>68.6</u>	0.136
Our Dark-ISP	**70.4**	0.136

5. Conclusion

We present Dark-ISP, a novel approach to RAW image processing for low-light object detection, leveraging physics-guided modular decomposition. Our key innovation lies in deconstructing conventional ISP pipelines into trainable linear sensor calibration and nonlinear tone mapping modules, preserving RAW data integrity while introducing task-driven content awareness. Our extensive experiments across various real-world and synthetic low-light datasets demonstrate that Dark-ISP outperforms state-of-the-art methods with fewer parameters, offering a lightweight yet powerful solution. By bridging the gap between physics-informed image processing and machine perception, Dark-ISP paves the way for more robust and generalizable visual systems that excel in low-light conditions and beyond. This approach also opens the door to broader applications in other perceptual tasks, such as segmentation, tracking, and even end-to-end autonomous driving.

References

[1] Qi Bi, Jingjun Yi, Hao Zheng, Wei Ji, Yawen Huang, Yuexiang Li, and Yefeng Zheng. Learning generalized medical image segmentation from decoupled feature queries. In *Proceedings of the AAAI Conference on Artificial Intelligence*, pages 810–818, 2024. 5

[2] Tim Brooks, Ben Mildenhall, Tianfan Xue, Jiawen Chen, Dillon Sharlet, and Jonathan T Barron. Unprocessing images for learned raw denoising. In *Proceedings of the IEEE/CVF conference on computer vision and pattern recognition*, pages 11036–11045, 2019. 2

[3] Zhaowei Cai and Nuno Vasconcelos. Cascade r-cnn: Delving into high quality object detection. In *2018 IEEE/CVF Conference on Computer Vision and Pattern Recognition*, 2018. 4

[4] Yue Cao, Ming Liu, Shuai Liu, Xiaotao Wang, Lei Lei, and Wangmeng Zuo. Physics-guided iso-dependent sensor noise modeling for extreme low-light photography. In *Proceedings of the IEEE/CVF Conference on Computer Vision and Pattern Recognition*, pages 5744–5753, 2023. 3

[5] Nicolas Carion, Francisco Massa, Gabriel Synnaeve, Nicolas Usunier, Alexander Kirillov, and Sergey Zagoruyko. End-to-end object detection with transformers. In *European conference on computer vision*, pages 213–229. Springer, 2020. 1

[6] Chen Chen, Qifeng Chen, Jia Xu, and Vladlen Koltun. Learning to see in the dark. In *Proceedings of the IEEE conference on computer vision and pattern recognition*, pages 3291–3300, 2018. 3, 6

[7] Chen Chen, Qifeng Chen, Minh N Do, and Vladlen Koltun. Seeing motion in the dark. In *Proceedings of the IEEE/CVF International conference on computer vision*, pages 3185–3194, 2019. 3

[8] Haoyu Chen, Jinjin Gu, Yihao Liu, Salma Abdel Magid, Chao Dong, Qiong Wang, Hanspeter Pfister, and Lei Zhu. Masked image training for generalizable deep image denoising. In *Proceedings of the IEEE/CVF Conference on Computer Vision and Pattern Recognition*, pages 1692–1703, 2023. 3

[9] Kai Chen, Jiaqi Wang, Jiangmiao Pang, Yuhang Cao, Yu Xiong, Xiaoxiao Li, Shuyang Sun, Wansen Feng, Ziwei Liu, Jiarui Xu, et al. Mmdetection: Open mmlab detection toolbox and benchmark. *arXiv preprint arXiv:1906.07155*, 2019. 5

[10] Linwei Chen, Ying Fu, Kaixuan Wei, Dezhi Zheng, and Felix Heide. Instance segmentation in the dark. *International Journal of Computer Vision*, 131(8):2198–2218, 2023. 1, 2, 6

[11] Wenshu Chen, Yujie Huang, Mingyu Wang, Xiaolin Wu, and Xiaoyang Zeng. Tsdn: Two-stage raw denoising in the dark. *IEEE Transactions on Image Processing*, 32:3679–3689, 2023. 3

[12] Xianmin Chen, Peiliang Huang, Xiaoxu Feng, Dingwen Zhang, Longfei Han, and Junwei Han. Retinex-rawmamba: Bridging demosaicing and denoising for low-light raw image enhancement. *arXiv preprint arXiv:2409.07040*, 2024. 3

[13] Marcos V Conde, Javier Vazquez-Corral, Michael S Brown, and Radu Timofte. Nilut: Conditional neural implicit 3d lookup tables for image enhancement. In *Proceedings of the AAAI Conference on Artificial Intelligence*, pages 1371–1379, 2024. 2

[14] Xiaohan Cui, Long Ma, Tengyu Ma, Jinyuan Liu, Xin Fan, and Risheng Liu. Trash to treasure: Low-light object detection via decomposition-and-aggregation. In *Proceedings of the AAAI Conference on Artificial Intelligence*, pages 1417–1425, 2024. 2

[15] Ziteng Cui and Tatsuya Harada. Raw-adapter: Adapting pretrained visual model to camera raw images. In *European Conference on Computer Vision*, pages 37–56. Springer, 2024. 1, 2, 3, 6, 8

[16] Ziteng Cui, Guo-Jun Qi, Lin Gu, Shaodi You, Zenghui Zhang, and Tatsuya Harada. Multitask aet with orthogonal tangent regularity for dark object detection. In *Proceedings of the IEEE/CVF international conference on computer vision*, pages 2553–2562, 2021. 2

[17] Rishit Dagli. Diffuseraw: End-to-end generative raw image processing for low-light images. *arXiv preprint arXiv:2402.18575*, 2023. 3

[18] Mauricio Delbracio, Damien Kelly, Michael S Brown, and Peyman Milanfar. Mobile computational photography: A tour. *Annual review of vision science*, 7(1):571–604, 2021. 2, 3, 4

[19] Steven Diamond, Vincent Sitzmann, Frank Julca-Aguilar, Stephen Boyd, Gordon Wetzstein, and Felix Heide. Dirty pixels: Towards end-to-end image processing and perception. *ACM Transactions on Graphics (TOG)*, 40(3):1–15, 2021. 3

[20] Xingbo Dong, Wanyan Xu, Zhihui Miao, Lan Ma, Chao Zhang, Jiewen Yang, Zhe Jin, Andrew Beng Jin Teoh, and Jiajun Shen. Abandoning the bayer-filter to see in the dark. In *Proceedings of the ieee/cvf conference on computer vision and pattern recognition*, pages 17431–17440, 2022. 3

[21] Zhipeng Du, Miaojing Shi, and Jiankang Deng. Boosting object detection with zero-shot day-night domain adaptation. In *Proceedings of the IEEE/CVF Conference on Computer Vision and Pattern Recognition*, pages 12666–12676, 2024. 2

[22] Gabriel Eilertsen, Rafał K Mantiuk, and Jonas Unger. Real-time noise-aware tone mapping. *ACM Transactions on Graphics (TOG)*, 34(6):1–15, 2015. 2

[23] Hansen Feng, Lizhi Wang, Yuzhi Wang, and Hua Huang. Learnability enhancement for low-light raw denoising: Where paired real data meets noise modeling. In *Proceedings of the 30th ACM International Conference on Multimedia*, pages 1436–1444, 2022. 3

[24] Ross Girshick. Fast r-cnn. In *Proceedings of the IEEE international conference on computer vision*, pages 1440–1448, 2015. 1

[25] Chunle Guo, Chongyi Li, Jichang Guo, Chen Change Loy, Junhui Hou, Sam Kwong, and Runmin Cong. Zero-reference deep curve estimation for low-light image enhancement. In *Proceedings of the IEEE/CVF conference on computer vision and pattern recognition*, pages 1780–1789, 2020. 2, 5, 8

[26] Haifeng Guo, Tong Lu, and Yirui Wu. Dynamic low-light image enhancement for object detection via end-to-end training. In *2020 25th International Conference on Pattern Recognition (ICPR)*, pages 5611–5618. IEEE, 2021. 2

[27] Yanhui Guo, Fangzhou Luo, and Xiaolin Wu. Learning degradation-independent representations for camera isp pipelines. In *Proceedings of the IEEE/CVF Conference on Computer Vision and Pattern Recognition*, pages 25774–25783, 2024. 2

[28] Khurram Azeem Hashmi, Goutham Kallempudi, Didier Stricker, and Muhammad Zeshan Afzal. Featenhancer: Enhancing hierarchical features for object detection and beyond under low-light vision. In *Proceedings of the IEEE/CVF International Conference on Computer Vision*, pages 6725–6735, 2023. 2, 6

[29] Kaiming He, Xiangyu Zhang, Shaoqing Ren, and Jian Sun. Deep residual learning for image recognition. In *Proceedings of the IEEE conference on computer vision and pattern recognition*, pages 770–778, 2016. 5

[30] Yang Hong, Kaixuan Wei, Linwei Chen, and Ying Fu. Crafting object detection in very low light. In *BMVC*, page 3, 2021. 2, 5

[31] Xin Jin, Ling-Hao Han, Zhen Li, Chun-Le Guo, Zhi Chai, and Chongyi Li. Dnf: Decouple and feedback network for seeing in the dark. In *Proceedings of the IEEE/CVF conference on computer vision and pattern recognition*, pages 18135–18144, 2023. 3

[32] Xin Jin, Jia-Wen Xiao, Ling-Hao Han, Chunle Guo, Ruixun Zhang, Xialei Liu, and Chongyi Li. Lighting every darkness in two pairs: A calibration-free pipeline for raw denoising. In *ICCV*, 2023. 3, 6

[33] Woohyeok Kim, Geonu Kim, Junyong Lee, Seungyong Lee, Seung-Hwan Baek, and Sunghyun Cho. Paramisp: learned forward and inverse isps using camera parameters. *arXiv preprint arXiv:2312.13313*, 2023. 2

[34] Ji Won Lee, Rae-Hong Park, and Soonkeun Chang. Local tone mapping using the k-means algorithm and automatic gamma setting. *IEEE Transactions on Consumer Electronics*, 57(1):209–217, 2011. 2

[35] Ruikang Li, Yujin Wang, Shiqi Chen, Fan Zhang, Jinwei Gu, and Tianfan Xue. Dualdn: Dual-domain denoising via differentiable isp. In *European Conference on Computer Vision*, pages 160–177. Springer, 2024. 2

[36] Tongxu Lin, Junyu Lin, Jingchao Wang, Zhengnan Deng, and Guoheng Huang. A dark transformation-equivariant algorithm for dark object detection. In *Proceedings of the 2023 4th International Conference on Computing, Networks and Internet of Things*, pages 731–735, 2023. 1, 2

[37] Tsung-Yi Lin, Michael Maire, Serge Belongie, James Hays, Pietro Perona, Deva Ramanan, Piotr Dollár, and C Lawrence Zitnick. Microsoft coco: Common objects in context. In *Computer vision–ECCV 2014: 13th European conference, zurich, Switzerland, September 6-12, 2014, proceedings, part v 13*, pages 740–755. Springer, 2014. 5, 6

[38] Tsung-Yi Lin, Priya Goyal, Ross Girshick, Kaiming He, and Piotr Dollár. Focal loss for dense object detection. In *Proceedings of the IEEE international conference on computer vision*, pages 2980–2988, 2017. 1, 5

[39] Xin Lin, Chao Ren, Xiao Liu, Jie Huang, and Yinjie Lei. Unsupervised image denoising in real-world scenarios via self-collaboration parallel generative adversarial branches. In *Proceedings of the IEEE/CVF International Conference on Computer Vision*, pages 12642–12652, 2023. 3

[40] William Ljungbergh, Joakim Johnander, Christoffer Petersson, and Michael Felsberg. Raw or cooked? object detection on raw images. In *Scandinavian Conference on Image Analysis*, pages 374–385. Springer, 2023. 2, 8

[41] Igor Morawski, Yu-An Chen, Yu-Sheng Lin, Shusil Dangi, Kai He, and Winston H Hsu. Genisp: Neural isp for low-light machine cognition. In *Proceedings of the IEEE/CVF Conference on Computer Vision and Pattern Recognition*, pages 630–639, 2022. 2, 5

[42] Ali Mosleh, Avinash Sharma, Emmanuel Onzon, Fahim Mannan, Nicolas Robidoux, and Felix Heide. Hardware-in-the-loop end-to-end optimization of camera image processing pipelines. In *Proceedings of the IEEE/CVF Conference on Computer Vision and Pattern Recognition*, pages 7529–7538, 2020. 2

[43] Daxin Peng, Wei Ding, and Tong Zhen. A novel low light object detection method based on the yolov5 fusion feature enhancement. *Scientific reports*, 14(1):4486, 2024. 2

[44] Haina Qin, Longfei Han, Juan Wang, Congxuan Zhang, Yanwei Li, Bing Li, and Weiming Hu. Attention-aware learning for hyperparameter prediction in image processing pipelines. In *European Conference on Computer Vision*, pages 271–287. Springer, 2022. 2

[45] Joseph Redmon, Santosh Divvala, Ross Girshick, and Ali Farhadi. You only look once: Unified, real-time object detection. In *Proceedings of the IEEE conference on computer vision and pattern recognition*, pages 779–788, 2016. 1

[46] Jihyun Seo, Hanse Ahn, Daewon Kim, Sungju Lee, Yongwha Chung, and Daihee Park. Embeddedpigdet—fast and accurate pig detection for embedded board implementations. *Applied Sciences*, 10(8):2878, 2020. 1

[47] Peize Sun, Rufeng Zhang, Yi Jiang, Tao Kong, Chenfeng Xu, Wei Zhan, Masayoshi Tomizuka, Lei Li, Zehuan Yuan, Changhu Wang, et al. Sparse r-cnn: End-to-end object detection with learnable proposals. In *Proceedings of the IEEE/CVF conference on computer vision and pattern recognition*, pages 14454–14463, 2021. 4

[48] Ashish Vaswani, Noam Shazeer, Niki Parmar, Jakob Uszkoreit, Llion Jones, Aidan N Gomez, Łukasz Kaiser, and Illia Polosukhin. Attention is all you need. *Advances in neural information processing systems*, 30, 2017. 4

[49] Tao Wang, Yong Li, Jingyang Peng, Yipeng Ma, Xian Wang, Fenglong Song, and Youliang Yan. Real-time image enhancer via learnable spatial-aware 3d lookup tables. In *Proceedings of the IEEE/CVF International Conference on Computer Vision*, pages 2471–2480, 2021. 2

[50] Yufei Wang, Yi Yu, Wenhan Yang, Lanqing Guo, Lap-Pui Chau, Alex C Kot, and Bihan Wen. Exposurediffusion: Learning to expose for low-light image enhancement. In *Proceedings of the IEEE/CVF International Conference on Computer Vision*, pages 12438–12448, 2023. 3

[51] Yujin Wang, Tianyi Xu, Zhang Fan, Tianfan Xue, and Jinwei Gu. Adaptiveisp: Learning an adaptive image signal pro-

cessor for object detection. *Advances in Neural Information Processing Systems*, 37:112598–112623, 2024. 2

[52] Yujin Wang, Tianyi Xu, Zhang Fan, Tianfan Xue, and Jinwei Gu. Adaptiveisp: Learning an adaptive image signal processor for object detection. *Advances in Neural Information Processing Systems*, 37:112598–112623, 2025. 2

[53] Kaixuan Wei, Ying Fu, Jiaolong Yang, and Hua Huang. A physics-based noise formation model for extreme low-light raw denoising. In *Proceedings of the IEEE/CVF Conference on Computer Vision and Pattern Recognition*, pages 2758–2767, 2020. 1, 3, 6

[54] Kaixuan Wei, Ying Fu, Yinqiang Zheng, and Jiaolong Yang. Physics-based noise modeling for extreme low-light photography. *IEEE Transactions on Pattern Analysis and Machine Intelligence*, page 1–1, 2021. 1, 6

[55] Yazhou Xing, Zian Qian, and Qifeng Chen. Invertible image signal processing. In *Proceedings of the IEEE/CVF conference on computer vision and pattern recognition*, pages 6287–6296, 2021. 2

[56] Wanyan Xu, Xingbo Dong, Lan Ma, Andrew Beng Jin Teoh, and Zhixian Lin. Rawformer: An efficient vision transformer for low-light raw image enhancement. *IEEE Signal Processing Letters*, 29:2677–2681, 2022. 3

[57] Xin Xu, Shiqin Wang, Zheng Wang, Xiaolong Zhang, and Ruimin Hu. Exploring image enhancement for salient object detection in low light images. *ACM transactions on multimedia computing, communications, and applications (TOMM)*, 17(1s):1–19, 2021. 1, 2

[58] Xinwei Xue, Jia He, Long Ma, Yi Wang, Xin Fan, and Risheng Liu. Best of both worlds: See and understand clearly in the dark. In *Proceedings of the 30th ACM International Conference on Multimedia*, pages 2154–2162, 2022. 1, 2

[59] Canqian Yang, Meiguang Jin, Yi Xu, Rui Zhang, Ying Chen, and Huaida Liu. Seplut: Separable image-adaptive lookup tables for real-time image enhancement. In *European Conference on Computer Vision*, pages 201–217. Springer, 2022. 2

[60] Masakazu Yoshimura, Junji Otsuka, Atsushi Irie, and Takeshi Ohashi. Dynamicisp: dynamically controlled image signal processor for image recognition. In *ICCV*. 2

[61] Syed Waqas Zamir, Aditya Arora, Salman Khan, Munawar Hayat, Fahad Shahbaz Khan, Ming-Hsuan Yang, and Ling Shao. Cycleisp: Real image restoration via improved data synthesis. In *Proceedings of the IEEE/CVF conference on computer vision and pattern recognition*, pages 2696–2705, 2020. 2

[62] Hui Zeng, Jianrui Cai, Lida Li, Zisheng Cao, and Lei Zhang. Learning image-adaptive 3d lookup tables for high performance photo enhancement in real-time. *IEEE Transactions on Pattern Analysis and Machine Intelligence*, 44(4), 2020. 2, 8

[63] Feng Zhang, Bin Xu, Zhiqiang Li, Xinran Liu, Qingbo Lu, Changxin Gao, and Nong Sang. Towards general low-light raw noise synthesis and modeling. In *Proceedings of the IEEE/CVF international conference on computer vision*, pages 10820–10830, 2023. 3

[64] Wenqiang Zhang, Tianheng Cheng, Xinggang Wang, Shaoyu Chen, Qian Zhang, and Wenyu Liu. Featurized query r-cnn. *arXiv preprint arXiv:2206.06258*, 2022. 4

[65] Yi Zhang, Hongwei Qin, Xiaogang Wang, and Hongsheng Li. Rethinking noise synthesis and modeling in raw denoising. In *Proceedings of the IEEE/CVF International Conference on Computer Vision*, pages 4593–4601, 2021. 3

[66] Yin Zhang, Yongqiang Zhang, Zian Zhang, Man Zhang, Rui Tian, and Mingli Ding. Isp-teacher: image signal process with disentanglement regularization for unsupervised domain adaptive dark object detection. In *Proceedings of the AAAI Conference on Artificial Intelligence*, pages 7387–7395, 2024. 2

[67] Xiang Zhu and Peyman Milanfar. Restoration for weakly blurred and strongly noisy images. In *2011 IEEE Workshop on Applications of Computer Vision (WACV)*, pages 103–109. IEEE, 2011. 2

[68] Xizhou Zhu, Weijie Su, Lewei Lu, Bin Li, Xiaogang Wang, and Jifeng Dai. Deformable detr: Deformable transformers for end-to-end object detection. *arXiv: Computer Vision and Pattern Recognition,arXiv: Computer Vision and Pattern Recognition*, 2020. 4